Regenerative Therapy 24 (2023) 528–535

Contents lists available at ScienceDirect

Regenerative Therapy

journal homepage: http://www.elsevier.com/locate/reth

Original Article

Raman spectroscopy to assess the differentiation of bone marrow mesenchymal stem cells into a glial phenotype

Sulei Bautista-González [a], Nidia Jannette Carrillo González [a], Tania Campos-Ordoñez [a], Mónica Alessandra Acosta Elías [b], Martín Rafael Pedroza-Montero [b, 1], Carlos Beas-Zárate [a], Graciela Gudiño-Cabrera [a, *]

[a] Laboratorio de Desarrollo y Regeneración Neural, Departamento de Biología Celular y Molecular, Centro Universitario de Ciencias Biológicas y Agropecuarias, Universidad de Guadalajara, Zapopan, Jalisco, Mexico
[b] Laboratorio de Biofísica Médica, Departamento de Investigación en Física, Universidad de Sonora, Hermosillo, Sonora, México

ARTICLE INFO

Article history:
Received 22 March 2023
Received in revised form
25 August 2023
Accepted 28 September 2023

Keywords:
Raman spectroscopy
Cell differentiation
Mesenchymal stem cells
conditioned medium
Glial phenotype

ABSTRACT

Background: Mesenchymal stem cells (MSCs) are multipotent precursor cells with the ability to self-renew and differentiate into multiple cell linage, including the Schwann-like fate that promotes regeneration after lesion. Raman spectroscopy provides a precise characterization of the osteogenic, adipogenic, hepatogenic and myogenic differentiation of MSCs. However, the differentiation of bone marrow mesenchymal stem cells (BMSCs) towards a glial phenotype (Schwann-like cells) has not been characterized before using Raman spectroscopy.
Method: We evaluated three conditions: 1) cell culture from rat bone marrow undifferentiated (uBMSCs), and two conditions of differentiation; 2) cells exposed to olfactory ensheathing cells-conditioned medium (dBMSCs) and 3) cells obtained from olfactory bulb (OECs). uBMSCs phenotyping was confirmed by morphology, immunocytochemistry and flow cytometry using antibodies of cell surface: CD90 and CD73. Glial phenotype of dBMSCs and OECs were verified by morphology and immunocytochemistry using markers of Schwann-like cells and OECs such as GFAP, p75 NTR and O4. Then, the Principal Component Analysis (PCA) of Raman spectroscopy was performed to discriminate components from the high wavenumber region between undifferentiated and glial-differentiated cells. Raman bands at the fingerprint region also were used to analyze the differentiation between conditions.
Results: Differences between Raman spectra from uBMSC and glial phenotype groups were noted at multiple Raman shift values. A significant decrease in the concentration of all major cellular components, including nucleic acids, proteins, and lipids were found in the glial phenotype groups. PCA analysis confirmed that the highest spectral variations between groups came from the high wavenumber region observed in undifferentiated cells and contributed with the discrimination between glial phenotype groups.
Conclusion: These findings support the use of Raman spectroscopy for the characterization of uBMSCs and its differentiation in the glial phenotype.

1. Introduction

Neurological disorders are the principal cause of disability and the second leading cause of death worldwide as consequence of the limited recovery capacity of the central nervous system (CNS) [1]. Functional and cognitive alterations become aggravated by the few therapeutic available options. Therefore, more effective treatments based on cellular therapy are needed to replace, or repair damaged tissue, and increase the functional restoration of the CNS [2,3]. Several studies in models of CNS injury and disease propose cell-based therapies using oligodendrocyte precursor cells (OPCs), Schwann cells (SCs), and olfactory ensheathing cells (OECs); however, those cells are difficult to harvest and to expand in vitro [2,4].

* Corresponding author.
E-mail address: graciela.gudino@academicos.udg.mx (G. Gudiño-Cabrera).
Peer review under responsibility of the Japanese Society for Regenerative Medicine.
[1] Deceased author.

https://doi.org/10.1016/j.reth.2023.09.016

Mesenchymal stem cells (MSCs) are considered a valuable alternative source for cell replacement therapies since they can be easily obtained from adult tissues and possess excellent self-renewing, proliferation, and multi-directional differentiation capabilities [5]. BMSCs had the potential to differentiate into Schwann-like cells with an induction efficiency calculated in approximately 97%, these cells develop a Schwann-like cell morphology and expressed several markers such as low-affinity nerve growth factor receptor (p75), glial fibrillary acidic protein (GFAP), S-100 and O4 [6]. Its differentiation in a glial phenotype helps to generate glial primary cell cultures and reduces complications of tumorigenesis during cell transplantation in damaged tissue [4]. Cell fate specification allows induce stem cells into glial differentiation exposing them to several factors including β-mercaptoethanol (β-ME) and all-trans retinoic acid (RA) followed cytokine cocktail including forskolin, bFGF, PDGF and neuregulin-1 [7]. Physiological microenvironment composition have also been studied including cell cocultures of MSCs with glial cells [8] and exposure of MSCs to OECs-conditioned medium (OECs-CM) [9,10].

The characterization of glial-differentiated MSCs is necessary to ensure the selection of the appropriate cell population prior to transplant. To detect specific proteins the commonly used approaches are immunocytochemistry or western blotting, which evidence co-expression of glial proteins (e.g. GFAP+, p75+, S100+) and a decreased expression of MSCs markers (e.g. CD90+, CD73+) [11,12]. However, both techniques are expensive and require a substantial number of cells for analysis and/or sample immunostaining, even more important their results are influenced by multiple parameters of the pre-analytical, analytical and post-analytical phases [13,14]. An alternative technique to asses cell differentiation is Raman spectroscopy which is an optical technique based on inelastic scattering of laser photons by molecular vibration of cellular molecules, which has raised interest in the field of biomedicine as it provides information of the cell chemical fingerprint with minimal sample manipulation (i.e. fixation, lysis or use of labels and other contrast enhancing chemicals) [15,16].

The cell differentiation process involves a series of changes that will result in a somatic functional unit; therefore, it is expected that a differential expression of specific biomolecules at various stages of differentiation will provide the key to discriminate between undifferentiated and differentiated cells [15]. Previously, Raman spectroscopy has been used to prove the osteogenic, adipogenic, hepatogenic and myogenic differentiation of MSCs [17–21]. However, information regarding the stem cell differentiation into a glial fate assessed by this technique remains scarce [22]. Thus, the aim of this study was to fully characterize the activity of cell culture rat bone marrow undifferentiated MSCs (uBMSCs), glial-differentiated MSCs (dBMSCs, exposed to OECs-CM) and OECs obtained from rat olfactory bulb by Principal Component Analysis (PCA) of Raman spectroscopy.

2. Materials and methods

2.1. Experimental animals and ethics statement

This work was performed using tissues obtained from Wistar rats (*Rattus norvegicus*, RRID: RGD_68115). Rodents were housed under optimal environmental conditions maintained in individual cages in a temperature-controlled room on a 12-h light/dark cycle with *ad libitum* access to food and water. All experiments were performed in accordance with the guidelines of the University of Guadalajara and Official Mexican regulations governing laboratory animal use (NOM-062-ZOO-1999 and NOM-033-ZOO-1995). The experimental procedures were designed to minimize the total number of animals used (n = 3) and the suffering of the animals. The animals were euthanized by CO_2 asphyxiation and immediately decapitated to extract the tissues for cultures.

2.2. Isolation and expansion of mesenchymal stem cells from bone marrow (BMSCs)

The BMSCs isolation culture was performed as previously described [22], briefly, the femur and tibia were dissected, the ends were cut at the level of the metaphysis and the bone marrow was obtained. After, this tissue passed under pressure the Hanks' solution with Ca^{2+} and Mg^{2+} and was centrifuged at 250 g for 7 min, the supernatant was removed and the cells were grown in medium supplemented with 10% FBS and kept under standard culture conditions in an atmosphere of 5% CO_2 and 36.5 °C. Cell viability was measured using the MTT assay (Invitrogen, Cat. M6494). At the second passage, the uBMSCs, dBMSCs and OECs were seeded in 96-well plates, after 3 days was added 20 μl of MTT (5 mg/ml) for 4 h of incubation. Finally, DMSO was added to dissolve the formazan crystals. Absorbance was measured at 590 nm (Supplementary Figure 1).

2.2.1. Immunophenotypic analyses of expressed antigens on cell surface

BMSCs characteristics were verified by morphology, adipogenic, chondrogenic and osteogenic differentiation potential using several mediums: Stem MACS AdipoDiff Media (Miltenyi Biotec, Cat. 130-091-677), StemMACS ChondroDiff Media (Miltenyi Biotec, Cat. 130-091-679) and StemMACS OsteoDiff Media (Miltenyi Biotec, Cat. 130-091-678) (Supplementary Figure 2). Further validation was done by immunocytochemistry and flow cytometry using antibodies of cell surface such as CD90 (Millipore, Cat. MAB1406, RRID: AB_11213488), CD73 (BD Pharmigen, Cat. 551123, RRID: AB_394057) and CD45 (BD Pharmigen, Cat. 554878, RRID: AB_395571). Data acquisition was performed in an Attune-NXT Acoustic Focusing Cytometer (Thermo Fisher Scientific) and analyzed with Kaluza Analysis 1.3 software. Three independent experiments were performed with three replicates in each case. For acquisition of each sample (10, 000, 000 events) we derived an initial dot-plot (FSC-A versus FSC-H) for singlets, then we performed a dot-plot analysis to define the region of uBMSCs with the combination of FSC-A versus SSC-A. Unstained cells in each channel were used to adjust the background fluorescence. Data were analyzed with Mini Tab 17 software. Average percentage of markers expression in the two groups were estimated. The complete information of antibodies is shown in the Supplementary table 1.

2.2.2. Immunocytochemistry

Cells were fixed with 4% paraformaldehyde (Sigma–Aldrich, Cat. P6148) for 8 min and washed prior to primary antibody incubation. As described above, to identify positive antigens on cell surface in cell with fibroblast-like morphology (undifferentiated cells), we used primary antibodies of cell surface (CD90 and CD73). In contrast, to analyze differentiated cells into a glial phenotype, we used primary antibodies such as mouse monoclonal IgG anti-p75NTR (Millipore, Cat. MAB365, RRID: AB_2152788), rabbit polyclonal IgG anti-GFAP (DAKO, Cat. Z0334, RRID: AB_10013382) and mouse monoclonal IgM anti-O4 (Millipore, Cat. MAB345, RRID: AB_11213138). All the antibodies were diluted 1:1000 in phosphate-buffered saline (PBS), pH 7.4, with 0.01% bovine serum albumin (Sigma–Aldrich, Cat. A9418). The incubation period with the anti-p75NTR and O4 antibodies were at least 16 h at 4 °C, whereas the incubation period with GFAP antibody was 1 h at room temperature. Next, the cells were incubated with a corresponding secondary antibody Alexa-Fluor 488-conjugated anti-mouse IgG antibody (Invitrogen, Cat. A21121, RRID: AB_141514), or Alexa-Fluor

594-conjugated anti-rabbit IgG antibody (Invitrogen, Cat. A-11012, RRID: AB_141359); those secondary antibodies were diluted 1:1000 in PBS and incubated for 45 min at room temperature. Then, cells were covered with a mounting solution (50% glycerol in PBS). Finally, we photographed cells under 40× objective using an Olympus BX53 fluorescence microscope with a Camera Micro-Plublisher 6 and Image Pro imaging software.

2.3. OECs culture and OECs-CM

Primary OECs cultures and OECs-CM obtainment were performed as previously described [23,24]. To acquire OECs-CM, purified OECs were maintained in medium supplemented with B-27 (Invitrogen, Cat. 17504-044).

2.3.1. Evaluation of the cell differentiation process

To confirm the glial differentiation status of BMSCs by Raman spectroscopy, after 72 h the glial expression was analyzed in three conditions: 1) uBMSCs maintained in medium supplemented with 10% FBS, 2) dBMSCs maintained in OECs-CM, and 3) OECs maintained in B-27. For Raman imaging, three different cell cultures were plated on sterilized calcium fluoride windows (CaF^2; 25 × 25 × 1 mm; Crystran Ltd.) and fixed with methanol (−20 °C, molecular grade), samples were kept at a −20 °C temperature until analysis. Data were recorded with an alpha300 RA Raman microscope (WITec) at a 532 nm excitation wavelength (CW continuous wave), a laser intensity of 10 mW/μm^2 and a 50× lens. Raman measurements were carried out with an accumulation time of 20 s. For each treatment five cells were selected and five spectra per cell were recorded. Then, spectra were pre-processed with Witec Control Software to perform background subtraction, baseline flattening and cosmic rays' removal. Raman spectroscopy data were averaged to obtain a single spectrum by using Excel (Microsoft Office) and then plotted with Origin Pro 8 software. Spectra were aligned to the phenylalanine peak at 1003 cm^{-1} before analysis.

2.4. Statistical analyses

Statistical assessment was performed using SPSS Statistics 20 (IBM Corp., Armonk, NY, USA) and GraphPad Prism 6 (GraphPad Software, Inc., La Jolla, CA, USA) statistical software. Data obtained from the three independent experiments were analyzed using one-way analysis of variance (ANOVA) with Bonferroni correction or Student's T-Test. Statistical significance was set at a value of $p < 0.05$.

3. Results

3.1. uBMSCs produces a fibroblast-like morphology and a high expression of CD73 and CD90

BMSCs were evaluated following the international criteria to define a MSCs that included the expression of cell surface markers and fibroblast-like in appearance [25]. The phenotypic characterization of the MSCs was done by immunocytochemistry and flow cytometry techniques. uBMSCs were adhered to plastic surface during the first 24 h of cell culture. Then, confluence was achieved after 7–10 days and cells were identified by the fibroblast-like morphology and positive expression of CD90 and CD73 by immunocytochemistry (Fig. 1A). In contrast, uBMSCs showed low stain of CD45 (Blank: Alexa 488) (Fig. 1A). Flow cytometry analysis confirmed that uBMSCs showed a high expression of CD90 (89.27% ± 3.64) and CD73 (56.10% ± 22.8) as compared to the minimum expression of the stem cell hematopoietic marker CD45

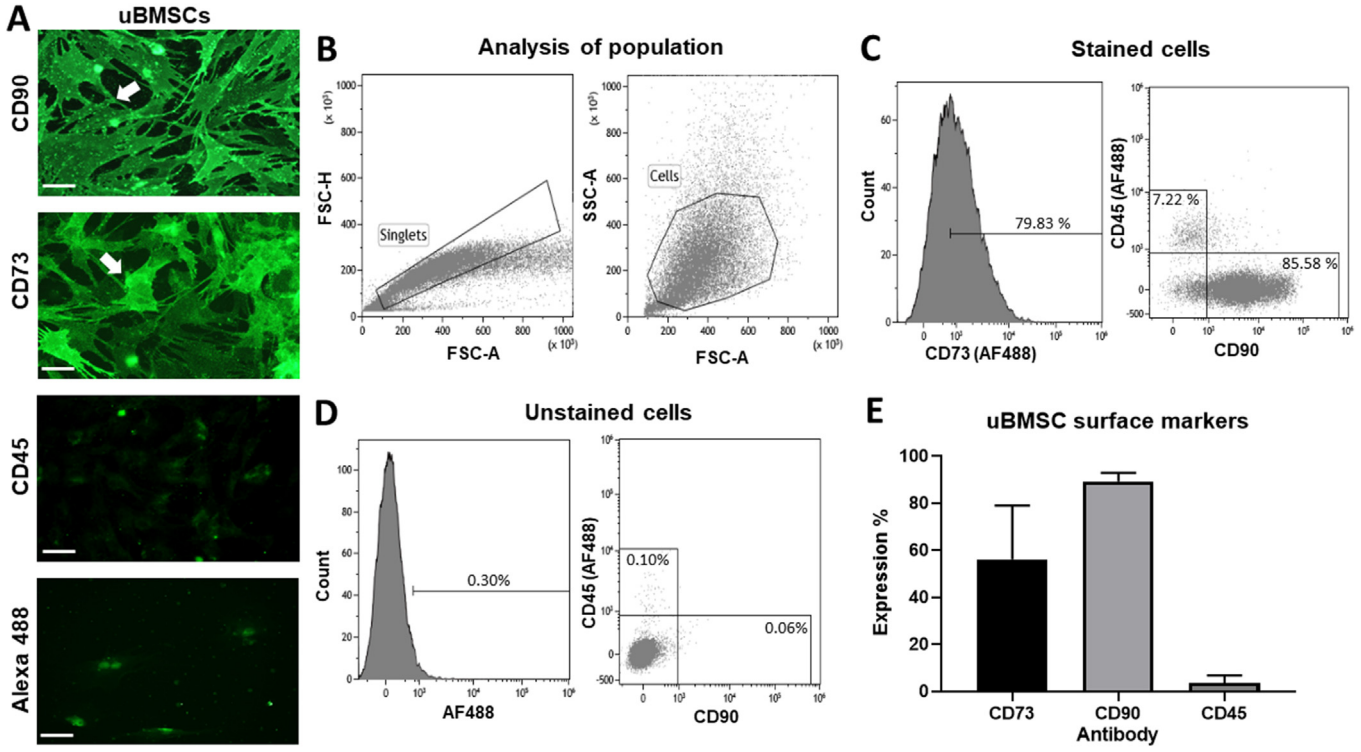

Fig. 1. Immunophenotypic characterization of rat bone marrow mesenchymal stem cells (BMSCs). (A) uBMSCs showed a fibroblast-like morphology (white arrows) and were positive for CD90 and CD73; and a scarce stain of CD45 and Alexa fluor 488 (AF488) were observed by immunocytochemistry, Bar: 50 μm. (B) Representative flow cytometry analysis of cell population was selected by prior elimination of duplicated events. Expression of CD73, CD45 and CD90 is shown in stained cells (C) and unstained cells (D). (E) uBMSCs show a high expression of CD73 and CD90 and a very low expression of CD45. BMSCs: bone marrow mesenchymal stem cells. FSC: forward scatter, SSC: side scatter.

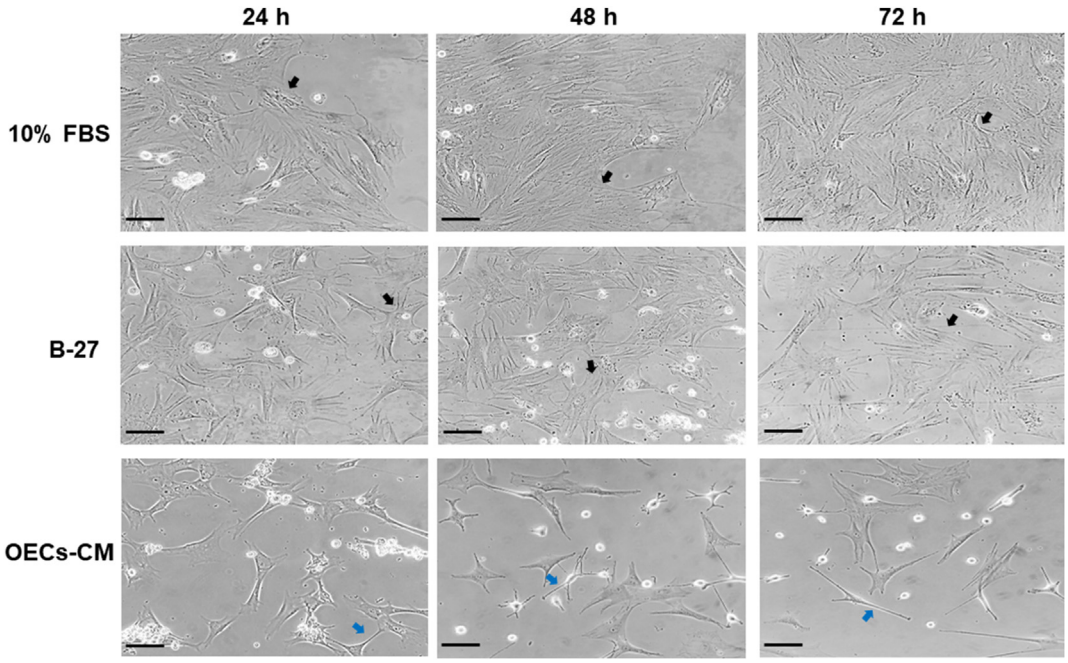

Fig. 2. BMSCs in vitro differentiation. MSCs culture evolution in three conditions is shown: 1) 10% FBS medium showed fibroblast shaped cells proliferated (black arrow), morphology was maintained during cell culture time, 2) B-27 medium showed similar fibroblast shaped morphology (black arrows), and 3) In OECs-CM medium a decrease in cell body size and development of elongated and thin cell projections were observed (blue arrows). Phase contrast microscopy, 10× magnification, Bar: 100 μm. OECs-CM: Olfactory Ensheathing Cell Conditioned Medium.

(3.65% ± 3.12, Fig. 1B–E). All values in the unstained cells were between 0.06 and 0.30%. These data indicate that uBMSCs group achieve the international criteria of MSCs.

3.2. uBMSCs produce a high amount of lipids, proteins and nucleic acids as compared to the glial phenotype groups

Differentiation of uBMSCs was performed by exposing cells to OECs-CM [26,27]. After 24 h of treatment, we found that BMSCs changed from a fibroblast-like morphology (Fig. 2, black arrows) to elongated spindle-shape and small cell body morphology (Fig. 2, blue arrows). These morphological changes were maintained after 48 h and 72 h (Fig. 2). Then, to verify the glial phenotype after the differentiation of BMSCs, we performed immunocytochemistry using markers of Schwann-like cells and OECs such as GFAP+ and p75NTR+. In Fig. 3, we characterized the uBMSCs with a fibroblast-like morphology (yellow arrow) and positive expression to CD90+ and GFAP+ (Fig. 3A). In contrast, dBMSCs showed small cell body,

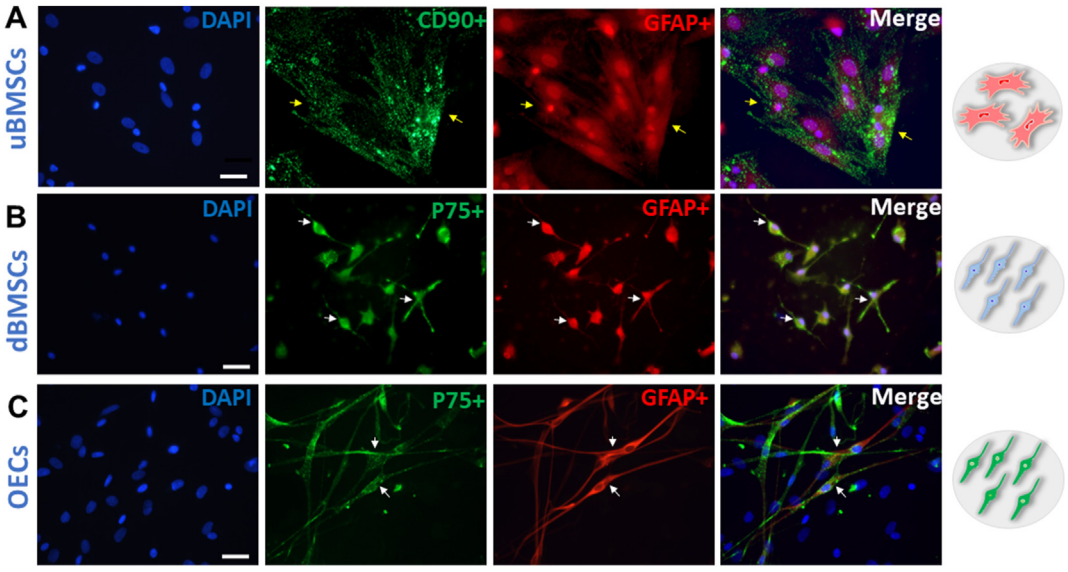

Fig. 3. Differentiated cell were identified by immunocytochemistry of p75NTR+ and GFAP+ antibodies. (A) uBMSCs showed a fibroblast-like morphology (yellow arrow) and positive expression to CD90+ and GFAP+. (B) dBMSCs showed elongated spindle-shape and small cell body morphology (white arrow) with positive expression to p75NTR+ and GFAP+. (C) OECs also showed elongated spindle-shape and small cell body morphology (white arrow) and positive expression to p75NTR+ and GFAP+. These data suggest that dBMSCs had a Schwann-like phenotype after the exposure to OECs-CM. Bar 50 μm.

elongated spindle-shape with a bipolar and multipolar morphology (white arrow) and positive expression to p75NTR+ and GFAP+ (Fig. 3B). Similarly, OECs showed elongated spindle-shape with bipolar structures, and small cell body (white arrow) and positive expression to p75NTR+ and GFAP+ (Fig. 3C). In the Supplementary material Fig. 3, we showed the positive expression to O4 and negative expression to CD90 antibodies in the glial phenotype groups, suggesting that the differentiated cells had a Schwann-like phenotype. Finally, to confirm the differentiation of uBMSCs into the glial phenotype we performed Raman spectroscopy and obtained spectra averages from three conditions. We observed in Fig. 4 that both groups of dBMSCs (blue line) and OECs (green line) showed similar number of peak locations as compared with uBMSCs (red line). The differences between Raman spectra from uBMSCs and dBMSCs were noted at multiple Raman shift values, with higher peak intensities in the group of uBMSCs (Fig. 4). These findings suggest that Raman spectroscopy is capable to discriminate between uBMSCs and its differentiation into a glial phenotype.

Then, we did a compressive characterization of fingerprint regions by group. uBMSCs group showed peaks related to lipid (514, 608 and 702 cm^{-1}) and nucleic acids (792 cm^{-1}, 1521 cm^{-1}). Higher peaks in this region were also observed at 1443 cm^{-1} and related to triglycerides and CH2 deformation of lipids and proteins; at 1209 cm^{-1} and 1228 cm^{-1} were associated with nucleic acids (T, A; ring breathing modes of the DNA/RNA bases) and proteins (amide III, tryptophan & phenylalanine n (C-C6H5)); at 1248, 1301, 1325 cm^{-1} and 1578 cm^{-1} were related to nucleic acids. In addition, uBMSCs showed more prominent peaks at 1003 cm^{-1} (phenylalanine), 1284 cm^{-1} (CH deformation of proteins) and 1647 cm^{-1} (amide I) (Fig. 4).

In the high wavenumber region, uBMSCs group showed two peaks at 2834 and 2940 cm^{-1} were prominent and merged with the single curve of dBMSCs with a shoulder at 2865 cm^{-1} and 2923 cm^{-1}. Raman bands at 2834 and 2865 cm^{-1} were associated with lipids, but bands at 2923 and 2940 cm^{-1} indicated protein relative amounts. Differentiated BMSCs and OECs groups showed similar peak location, but more intensities and peaks located at 1578 and 1711 cm^{-1} were observed in the dBMSCs group as compared with OECs (Fig. 4). Assignment of Raman Bands are complete described in the Supplementary Table 2.

Principal Component Analysis (PCA) was performed to understand the spectral variation between groups which are shown as clusters in Fig. 5. The first two components (PCs) contained 95% of variance in the combined data. PC1 allowed to separate uBMSCs from the rest of the groups, PC1 accounted for 85% of the variance mostly due to the region between 2500 and 3200 cm^{-1}, but spectral variations also was associated with peaks in fingerprint region of Amide I, Amide III, phenylalanine, adenine, phosphatidylinositol and cholesterol. In contrast, PC2 that represented 10% of the variance showed an overlap between OECs and dBMSCs groups at the high wavenumber region on peaks related to lipids and protein content, but also were peaks in the fingerprint region associated with phosphatidylinositol and cholesterol content (Fig. 5). These data suggest that uBMSCs are characterized by two prominent peaks in the high wavenumber region that indicate a high amount of lipids and proteins as compared with glial phenotype groups.

4. Discussion

Herein, we evaluated three conditions of cell culture from rat bone marrow undifferentiated BMSCs, glial-differentiated MSCs (dBMSCs, exposed to olfactory ensheathing cells-conditioned medium OECs-CM), and OECs obtained from olfactory bulb (as a control). First, uBMSCs phenotyping was verified by morphology, immunocytochemistry and flow cytometry using cell surface antibodies CD90 and CD73. Then, we evaluated the effectiveness of Raman spectroscopy to discriminate between undifferentiated and glial-differentiated cells. Our data indicate that uBMSCs showed fibroblast-like morphology and a high expression of CD73 and CD90. Glial phenotype groups showed elongated spindle-shape with bipolar and multipolar structures and small cell body morphology and the expression of GFAP, p75NTR and O4 proteins. Differences between Raman spectra from uBMSC and glial phenotype groups were noted at multiple Raman shift values. A significant decrease in the concentration of all major cellular components, including nucleic acids, proteins, and lipids were found in the glial phenotype groups. PCA analysis confirmed that the highest spectral variations between groups came from the high wavenumber region observed in undifferentiated cells and contributed with the discrimination between glial phenotype groups.

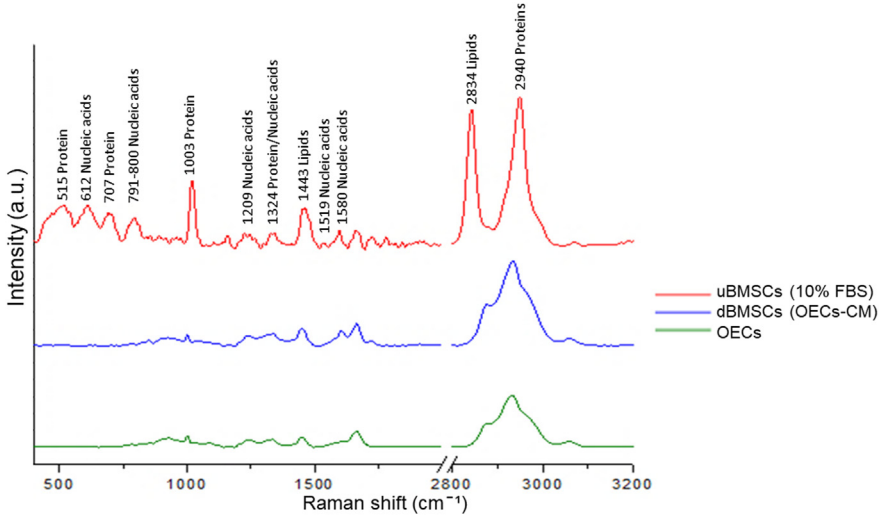

Fig. 4. BMSCs glial differentiation by Raman spectroscopy. Spectra from each group represents the mean of 5 measures from five different cells. Raman shift includes the fingerprint region (600–1800 cm^{-1}) and high wavenumber region (2500–3200 cm^{-1}). Values from 2000 to 2800 cm^{-1} were cut for illustrative means. Raman spectra of BMSCs before and after cell differentiation exhibited great modifications in the fingerprint region and the high wavenumber region. In contrast, differentiated groups (OECs and BMSCs exposed to OECs-CM) showed a similar Raman spectra with differences in peak intensities and a prominent Raman peak at 1610 cm^{-1}, which is maintained after cell differentiation. Intensity values are represented in arbitrary units (a.u.). OECs: Olfactory Ensheathing Cells. BMSCs: Bone Marrow Mesenchymal Stem Cells.

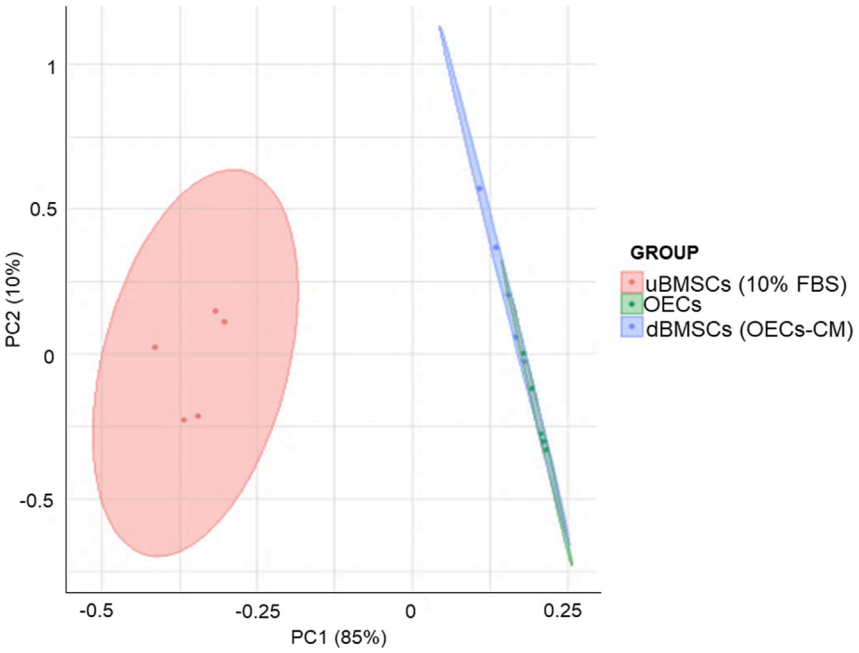

Fig. 5. Principal Component Analysis of glial differentiation of BMSCs. PCA showed different distribution and scores between undifferentiated BMSCs, OECs and uBMSCs after 72 h of treatment. BMSCs: Bone Marrow Mesenchymal Stem Cells. OECs: Olfactory Ensheathing Cells.

Stem cells are endowed with self-renewal capability and has been proposed as a replacement therapy in recovery from spinal cord injury and neurodegenerative diseases. Schwann cells play pivotal roles in regenerating damaged nerve, and their use in clinical cell-based therapy is hampered due to its limited availability and the effectiveness of a protocol for MSCs transdifferentiation into a Schwann cells lineage has been questioned before [28]. According to the Mesenchymal and Tissue Stem Cell Committee of the International Society for Cellular Therapy, MSCs can be defined by 3 main criteria: 1) adherence to plastic culture ware; 2) expression of surface proteins such as CD90, CD73, and CD105 and lack of expression of CD45, CD34, CD14 or CD11b, CD79a or CD19, and HLA class II; 3) the ability to differentiate into osteoblasts, adipocytes, and chondroblasts when they are cultured in a specific differentiating media. In this study, we found that uBMSCs showed plastic adherence after 24 h in vitro and had the ability to differentiate into osteoblasts, and adipocytes. Also, these cells were positive for CD90 and CD73 and were negative to the hematopoietic marker CD45. Therefore, our results suggest that uBMSCs followed the international criteria to define a murine MSCs.

Different approaches have been used to direct MSCs differentiation toward diverse cell fates, including those outside the mesenchymal lineage. One technique to induce the differentiation of MSCs is their exposure to OECs-CM, which contain several extrinsic signaling molecules such as growth factors, neurotrophic factors, and cell adhesion molecules among other substances [10,29–32]. OECs-CM seem to be sufficient to benefit the expression of genes involved in the cell phenotype, neurite outgrowth promotion and myelination when applied to stem cells [26,33]. We found that bone marrow MSCs treated with OECs-CM were differentiated into Schwann-like cells with morphological changes towards an elongating spindle shape and antigenic phenotype characteristic of glial cells [34]. Indeed, these cells expressed GFAP, p75NTR and O4 proteins after 72 h of treatment that also are characteristics of Schwann-like cells [35]. Thus, our results suggest that differentiated cells, dBMSCs and OECs showed typical characteristics of glial cells.

Raman spectroscopy provides quantitative and qualitative information regarding the biochemical features of a sample. Raman shift in biological samples ranges from 600 cm^{-1} to 1 to 3200 cm^{-1} and is divided into three spectral regions: 1) fingerprint region is specific to identify larger atoms such as carbon, nitrogen, and oxygen or complexes of several hydrogen atoms (600–1800 cm^{-1}); 2) silent region detect alkynes (1800–2500 cm^{-1}); and 3) high wavenumber region detect hydrogen atoms vibrating with high energies in comparison with other bonds such as CH, NH and OH stretching of lipids and proteins (2500–3400 cm^{-1}) [16,36–39]. In our study, uBMSCs showed typical peaks at the fingerprint region related to the major components in cells, these results are similar to previous studies of MSC from bone marrow, umbilical cord, and mammalian cell lines [36,37]. In contrast, there is little information on Raman spectra regarding single neural cells. Morisaki et al. studied rat sciatic nerve Schwann cells and found prominent peaks at 2851 cm^{-1}, 2885 cm^{-1}, 2909 cm^{-1} and 2919 cm^{-1}, which are associated with CH2 vibrations modes and lipid content, they concluded that the observed peaks reflect the composition of myelin [40]. In addition, also neurites of Dorsal Root Ganglions showed prominent peak at 2940 cm^{-1}, which is related to CH3 symmetric stretching and reflects protein content [40]. To the best of our knowledge, the differentiation of BMSCs towards a glial phenotype by Raman has not been described before. Thus, our results suggest that differentiated cells, dBMSCs and OECs groups showed weaker peaks at the fingerprint region in comparison to the single curve at 2923 cm^{-1} in the high wavenumber region similar to other neural cells.

In addition, when a cell has a differentiation process will result in a Raman shift as compared to its undifferentiated state. For example, the differentiation of MSCs to an osteogenic lineage result in the development of a peak at 960 cm^{-1} which is associated to the symmetric stretch vibration of hydroxyapatite and the presence of phosphates associated with mineralization in osteo cells [17–19]; on the other hand, a stronger peak at 2900 cm^{-1} or at 2935 cm^{-1} are representative of the abundance of fatty acidic peak and abundance of lipid droplets, as the main characteristics of the

differentiation of MSCs into adipocytes, both of which are distinguishable with the Raman peaks of MSCs [20,41]. The differentiation of MSCs to chondrocytes result in 867, 1065 and 1437 cm^{-1} bands associated with vibrations of hydroxyproline (collagen) and CH2 deformation from lipids content [42–44]. Hepatic differentiation from the MSCs showed a prominent peak at 1750 cm^{-1} assigned to triacylglicerols [45], or another peak at 2800–3000 cm^{-1}, which is associated with glycosidic bonds as compared with the Raman peaks of undifferentiated MSCs [21]. In our study, dBMSCs and OECs groups showed a low shoulder at 2865 cm^{-1} but a single curve at 2923 cm^{-1} in the high wavenumber region related to lipids and protein content, in contrast, uBMSCs group develops two prominent peaks at 2834 and 2940 cm^{-1} associated with CH2 symmetric stretch of lipids and CH3 symmetric of proteins. These sites of curves appear similar between groups, but the changes were noted at multiple Raman shift values and intensity shifts. These results suggest a significant decrease in the concentration of all major cellular components, including nucleic acids, proteins, and lipids during the differentiation process in the dBMSCs and OECs groups. Furthermore, a higher number of peaks and Raman shifts with stronger curves related to lipids, cell membrane composition and energy storage functions were found along the Raman spectra in the uBMSC group. Lipids play an important role in cells such as structural and protective elements, source of energy and mediators of the activation of several signaling pathways. Previous, a low lipid content has been reported during differentiation in stem cells. Heraud et al. showed that undifferentiated hESC displayed higher lipid and glycogen levels when compared to their differentiated state into cells committed to mesendoderm or ectoderm [46]. Moreover, Pijanka et al. demonstrated that Raman bands associated to lipids show a minor elevation in human MSC when compared to human Embryonic Stem Cells [47]. These results in the Raman shifts could be related to a less capacity in cells to differentiate as they become more specialized. In addition, higher signals of Raman bands were related to the content of nucleic acids and proteins in primary and immortalized cells. Ghita et al. found that the main spectral differences between groups were higher in the Neural Stem Cells (NSC) than in glial phenotype [15]. In our study, uBMSCs possess a high proliferation capacity, thus, the higher peaks could be due to their proliferative condition in comparison with glial-differentiated groups. PCA showed that the highest spectral variations between groups came from the high wavenumber region of uBMSCs and contributed with the discrimination analysis between cell groups. Moreover, this analysis is helpful to detect similar biochemical features among glial phenotypes groups. Nevertheless, future studies are needed to strengthen a complete characterization of the differentiation of bone marrow derived mesenchymal stem cells into a glial phenotype by OECs-CM, it is required marker-based analyzing methods such as quantitative PCR, western blotting, flow cytometry, functional assessment, parallel single-cell RNA-seq or in situ hybridization. Finally, these findings support the use of Raman spectroscopy technology for characterization of MSCs and its differentiation into a glial phenotype. We propose that the criteria to evaluate the differentiation of MSCs may include a structural and functional characterization by Raman spectroscopy technology.

Author contributions

Conception and design of experiments: GGC, SBG, MAE. Reagents and samples: GGC and CBZ. Execution of experiments: GGC, SBG. Interpretation and writing of manuscript: GGC, SBG, NJCG, TCO and CBZ. The manuscript has been read and approved by all named authors.

Funding

This study was funded by grants from the National Council of Science and Technology of Mexico (CONACyT No. CB-01-2012-177594) for GGC and CBZ; and the CONACyT No. CB-01-2012-181779 for GGC. Bautista-González Sulei was supported by the doctoral fellowship (CONACyT No. 185241).

Declaration of competing interest

The authors declare no conflict of interest.

Acknowledgments

The authors thank Dr. Pablo Ortíz Lazareno for the guidance in the flow cytometry experiments, also to Dr. Raúl Riera Aroche for the contact to the Universidad de Sonora. We would like to manifest our appreciation to Miguel Angel Nuñez Ochoa for the invaluable statistical analysis of the principal component and Gabriela Escobar Camberos for the technical support.

Appendix A. Supplementary data

Supplementary data to this article can be found online at https://doi.org/10.1016/j.reth.2023.09.016.

References

[1] Feigin VL, Vos T, Nichols E, Owolabi MO, Carroll WM, Dichgans M, et al. The global burden of neurological disorders: translating evidence into policy. Lancet Neurol 2020;19(3):255–65. https://doi.org/10.1016/S1474-4422(19)30411-9.
[2] Manganas LN, Maletic-Savatic M. Stem cell therapy for CNS demyelinating disease. Natl Inst Health 2005;29(3):225–31. https://doi.org/10.1016/j.biotechadv.2011.08.021.Secreted.
[3] Rowland JW, Hawryluk GWJ, Kwon B, Fehlings MG. Current status of acute spinal cord injury pathophysiology and emerging therapies: promise on the horizon. Neurosurg Focus 2008;25(5):E2. https://doi.org/10.3171/foc.2008.25.11.e2.
[4] Yang J, Rostami A, Zhang GX. Cellular remyelinating therapy in multiple sclerosis. J Neurol Sci 2009;276(1–2):1–5. https://doi.org/10.1016/j.jns.2008.08.020.
[5] Kobolak J, Dinnyes A, Memic A, Khademhosseini A, Mobasheri A. Mesenchymal stem cells: identification, phenotypic characterization, biological properties and potential for regenerative medicine through biomaterial micro-engineering of their niche. Methods 2016;99:62–8. https://doi.org/10.1016/j.ymeth.2015.09.016.
[6] Wakao S, Matsuse D, Dezawa M. Mesenchymal stem cells as a source of schwann cells: their anticipated use in peripheral nerve regeneration. Cells Tissues Organs 2014;200(1):31–41. https://doi.org/10.1159/000368188.
[7] Pan Y, Cai S. Current state of the development of mesenchymal stem cells into clinically applicable Schwann cell transplants. Mol Cell Biochem 2012;368(1–2):127–35. https://doi.org/10.1007/s11010-012-1351-6.
[8] Wang B, Han J, Gao Y, Xiao Z, Chen B, Wang X, et al. The differentiation of rat adipose-derived stem cells into OEC-like cells on collagen scaffolds by co-culturing with OECs. Neurosci Lett 2007;421(3):191–6. https://doi.org/10.1016/j.neulet.2007.04.081.
[9] Feng L, Gan H, Zhao W, Liu Y. Effect of transplantation of olfactory ensheathing cell conditioned medium induced bone marrow stromal cells on rats with spinal cord injury. Mol Med Rep 2017;16(2):1661–8. https://doi.org/10.3892/mmr.2017.6811.
[10] Lo Furno D, Pellitteri R, Graziano ACE, Giuffrida R, Vancheri C, Gili E, et al. Differentiation of human adipose stem cells into neural phenotype by neuroblastoma- or olfactory ensheathing cells-conditioned medium. J Cell Physiol 2013;228(11):2109–18. https://doi.org/10.1002/jcp.24386.
[11] Brohlin M, Mahay D, Novikov LN, Terenghi G, Wiberg M, Shawcross SG, et al. Characterisation of human mesenchymal stem cells following differentiation into Schwann cell-like cells. Neurosci Res 2009;64(1):41–9. https://doi.org/10.1016/j.neures.2009.01.010.
[12] Mahay D, Terenghi G, Shawcross SG. Growth factors in mesenchymal stem cells following glial-cell differentiation. Biotechnol Appl Biochem 2008;51(4):167. https://doi.org/10.1042/ba20070212.
[13] Hnasko TS, Hnasko RM. The western blot. In: Hnasko R, editor. Methods in molecular biology. New York, NY: Humana Press; 2015. p. 87–96. https://doi.org/10.1007/978-1-4939-2742-5_9.

[14] Im K, Mareninov S, Diaz MFP, Yong WH. An introduction to performing immunofluorescence staining. Methods Mol Biol 2019;1897:299–311. https://doi.org/10.1007/978-1-4939-8935-5_26.
[15] Ghita A, Pascut FC, Sottile V, Denning C, Notingher I. Applications of Raman micro-spectroscopy to stem cell technology: label-free molecular discrimination and monitoring cell differentiation. EPJ Tech Instrum 2015;2(1). https://doi.org/10.1140/epjti/s40485-015-0016-8.
[16] Shipp DW, Sinjab F, Notingher I. Raman spectroscopy: techniques and applications in the life sciences. Adv Opt Photon 2017;9(2):315. https://doi.org/10.1364/aop.9.000315.
[17] McManus LL, Burke GA, McCafferty MM, O'Hare P, Modreanu M, Boyd AR, et al. Raman spectroscopic monitoring of the osteogenic differentiation of human mesenchymal stem cells. Analyst 2011;136(12):2471–81. https://doi.org/10.1039/c1an15167c.
[18] Molony C, McIntyre J, Maguire A, Hakimjavadi R, Burtenshaw D, Casey G, et al. Label-free discrimination analysis of de-differentiated vascular smooth muscle cells, mesenchymal stem cells and their vascular and osteogenic progeny using vibrational spectroscopy. Biochim Biophys Acta Mol Cell Res 2018;1865(2):343–53. https://doi.org/10.1016/j.bbamcr.2017.11.006.
[19] Salehi H, Collart-Dutilleul P-Y, Gergely C, Cuisinier FJG. Confocal Raman microscopy to monitor extracellular matrix during dental pulp stem cells differentiation. J Biomed Opt 2015;20(7):076013. https://doi.org/10.1117/1.jbo.20.7.076013.
[20] Suhito IR, Han Y, Min J, Son H, Kim TH. In situ label-free monitoring of human adipose-derived mesenchymal stem cell differentiation into multiple lineages. Biomaterials 2018;154:223–33. https://doi.org/10.1016/j.biomaterials.2017.11.005.
[21] Wu HH, Ho JH, Lee OK. Detection of hepatic maturation by Raman spectroscopy in mesenchymal stromal cells undergoing hepatic differentiation. Stem Cell Res Ther 2016;7(1). https://doi.org/10.1186/s13287-015-0259-y.
[22] Huang S, Xu L, Sun Y, Wu T, Wang K, Li G. An improved protocol for isolation and culture of mesenchymal stem cells from mouse bone marrow. J Orthop Translat 2015;3(1):26–33. https://doi.org/10.1016/j.jot.2014.07.005.
[23] Chandler CE, Parsons LM, Hosang M, Shooter EM. A monoclonal antibody modulates the interaction of nerve growth factor with PC12 cells. J Biol Chem 1984;259(11):6882–9.
[24] Gudiño-Cabrera G, Nieto-Sampedro M, Gudino-Cabrera G, Nieto-Sampedro M. Ensheathing cells: large scale purification from adult olfactory bulb, freeze-preservation and migration of transplanted cells in adult brain. Restor Neurol Neurosci 1996;10(1):25–34. https://doi.org/10.3233/RNN-1996-10104.
[25] Samsonraj RM, Raghunath M, Nurcombe V, Hui JH, van Wijnen AJ, Cool SM. Concise review: multifaceted characterization of human mesenchymal stem cells for use in regenerative medicine. Stem Cells Transl Med 2017;6(12):2173–85. https://doi.org/10.1002/sctm.17-0129.
[26] Doncel-Pérez E, Caballero-Chacón S, Nieto-Sampedro M. Neurosphere cell differentiation to aldynoglia promoted by olfactory ensheathing cell conditioned medium. Glia 2009;57(13):1393–409. https://doi.org/10.1002/glia.20858.
[27] Ponce-Regalado MD, Ortuño-Sahagún D, Zarate CB, Gudiño-Cabrera G. Ensheathing cell-conditioned medium directs the differentiation of human umbilical cord blood cells into aldynoglial phenotype cells. Hum Cell 2012;25(2):51–60. https://doi.org/10.1007/s13577-012-0044-5.
[28] Movaghar B, Tiraihi T, Mesbah-Namin SA. Transdifferentiation of bone marrow stromal cells into Schwann cell phenotype using progesterone as inducer. Brain Res 2008;1208:17–24. https://doi.org/10.1016/j.brainres.2008.02.071.
[29] Choi D, Gladwin K. Olfactory ensheathing cells: Part ii - source of cells and application to patients. World Neurosurgery 2015;83(2):251–6. https://doi.org/10.1016/j.wneu.2013.07.016.
[30] Lo Furno D, Mannino G, Giuffrida R, Gili E, Vancheri C, Tarico MS, et al. Neural differentiation of human adipose-derived mesenchymal stem cells induced by glial cell conditioned media. J Cell Physiol 2018;233(10):7091–100. https://doi.org/10.1002/jcp.26632.
[31] Sethi R, Sethi R, Redmond A, Lavik E. Olfactory ensheathing cells promote differentiation of neural stem cells and robust neurite extension. Stem Cell Rev Reports 2014;10(6):772–85. https://doi.org/10.1007/s12015-014-9539-7.
[32] Silva NA, Gimble JM, Sousa N, Reis RL, Salgado AJ. Combining adult stem cells and olfactory ensheathing cells: the secretome effect. Stem Cell Dev 2013;22(8):1232–40. https://doi.org/10.1089/scd.2012.0524.
[33] Rojas-Mayorquín AE, Torres-Ruíz NM, Ortuño-Sahagún D, Gudiño-Cabrera G. Microarray analysis of striatal embryonic stem cells induced to differentiate by ensheathing cell conditioned media. Dev Dynam 2008;237(4):979–94. https://doi.org/10.1002/dvdy.21489.
[34] Wang B, Zhao Y, Lin H, Chen B, Zhang J, Zhang J, et al. Phenotypical analysis of adult rat olfactory ensheathing cells on 3-D collagen scaffolds. Neurosci Lett 2006;401(1–2):65–70. https://doi.org/10.1016/j.neulet.2006.02.085.
[35] Gudiño-Cabrera G, Nieto-Sampedro M. Schwann-like macroglia in adult rat brain. Glia 2000;30(1):49–63. https://doi.org/10.1002/(SICI)1098-1136(200003)30:1<49::AID-GLIA6>3.0.CO;2-M.
[36] Bai H, Li H, Han Z, Zhang C, Zhao J, Miao C, et al. Label-free assessment of replicative senescence in mesenchymal stem cells by Raman microspectroscopy. Biomed Opt Express 2015;6(11):4493. https://doi.org/10.1364/boe.6.004493.
[37] Kim BS, Lee CCI, Christensen JE, Huser TR, Chan JW, Tarantal AF. Growth, differentiation, and biochemical signatures of rhesus monkey mesenchymal stem cells. Stem Cell Dev 2008;17(1):185–98. https://doi.org/10.1089/scd.2007.0076.
[38] Matthäus C, Krafft C, Dietzek B, Brehm BR, Lorkowski S, Popp J. Noninvasive imaging of intracellular lipid metabolism in macrophages by Raman microscopy in combination with stable isotopic labeling. Anal Chem 2012;84(20):8549–56. https://doi.org/10.1021/ac3012347.
[39] Movasaghi Z, Rehman S, Rehman IU. Raman spectroscopy of biological tissues. Appl Spectrosc Rev 2007;42(5):493–541. https://doi.org/10.1080/05704920701551530.
[40] Morisaki S, Ota C, Matsuda K, Kaku N, Fujiwara H, Oda R, et al. Application of Raman spectroscopy for visualizing biochemical changes during peripheral nerve injury in vitro and in vivo. J Biomed Opt 2013;18(11):116011. https://doi.org/10.1117/1.JBO.18.11.116011.
[41] Suhito IR, Han Y, Ryu YS, Son H, Kim TH. Autofluorescence-Raman Mapping Integration analysis for ultra-fast label-free monitoring of adipogenic differentiation of stem cells. Biosens Bioelectron 2021;178(November 2020):113018. https://doi.org/10.1016/j.bios.2021.113018.
[42] Lazarević JJ, Kukolj T, Bugarski D, Lazarević N, Bugarski B, Popović ZV. Probing primary mesenchymal stem cells differentiation status by micro-Raman spectroscopy. Spectrochim Acta Mol Biomol Spectrosc 2019;213:384–90. https://doi.org/10.1016/j.saa.2019.01.069.
[43] Ravera F, Efeoglu E, Byrne HJ. Monitoring stem cell differentiation using Raman microspectroscopy: chondrogenic differentiation, towards cartilage formation. Analyst 2021;146(1):322–37. https://doi.org/10.1039/d0an01983f.
[44] Votteler M, Carvajal Berrio DA, Pudlas M, Walles H, Schenke-Layland K. Non-contact, label-free monitoring of cells and extracellular matrix using Raman spectroscopy. JoVE 2012;63:1–7. https://doi.org/10.3791/3977.
[45] Paramitha PN, Zakaria R, Maryani A, Kusaka Y, Andriana BB, Hashimoto K, et al. Raman study on lipid droplets in hepatic cells co-cultured with fatty acids. Int J Mol Sci 2021;22(14). https://doi.org/10.3390/ijms22147378.
[46] Heraud P, Ng ES, Caine S, Yu QC, Hirst C, Mayberry R, et al. Fourier transform infrared microspectroscopy identifies early lineage commitment in differentiating human embryonic stem cells. Stem Cell Res 2010;4(2):140–7. https://doi.org/10.1016/j.scr.2009.11.002.
[47] Pijanka JK, Kumar D, Dale T, Yousef I, Parkes G, Untereiner V, et al. Vibrational spectroscopy differentiates between multipotent and pluripotent stem cells. Analyst 2010;135(12):3126. https://doi.org/10.1039/c0an00525h.